J Physiol 588.13 (2010) pp 2315–2328

The Journal of Physiology

Stimulation of human and mouse erythrocyte Na^+–K^+–$2Cl^-$ cotransport by osmotic shrinkage does not involve AMP-activated protein kinase, but is associated with STE20/SPS1-related proline/alanine-rich kinase activation

Brice Sid[1], Lisa Miranda[1], Didier Vertommen[1], Benoît Viollet[2] and Mark H. Rider[1]

[1] *Université catholique de Louvain and de Duve Institute, Avenue Hippocrate, 74, B-1200 Brussels, Belgium*
[2] *Institut Cochin, Université Paris Descartes, CNRS (UMR 8104) and INSERM U567, Department of Endocrinology, Metabolism and Cancer, Paris, France*

This study was undertaken to investigate whether the mechanism of increased Na^+–K^+–$2Cl^-$ (NKCC1) cotransporter activity by osmotic shrinkage involved AMP-activated protein kinase (AMPK) activation. AMPK was found to phosphorylate a recombinant GST-dogfish (1–260) NKCC1 fragment at Ser38 and Ser214, corresponding to Ser77 and Ser242 in human NKCC1, respectively. Incubation of human erythrocytes with 20 μM A769662 AMPK activator increased Ser242 NKCC1 phosphorylation but did not stimulate $^{86}Rb^+$ uptake. Under hypertonic conditions in human red blood cells (RBCs) incubated with 0.3 M sucrose, NKCC1 activity increased as measured by bumetanide-sensitive $^{86}Rb^+$ uptake and AMPK was activated. However, there was no effect of AMPKα1 deletion in mouse RBCs on the increased rate of $^{86}Rb^+$ uptake induced by hyperosmolarity. AMPK activation by osmotic shrinkage of mouse RBCs was abrogated by 10 μM STO-609 CaMKKβ inhibitor, but incubation with STO-609 did not affect the increase in $^{86}Rb^+$ uptake induced by hyperosmolarity. Osmotic shrinkage of human and mouse RBCs led to activation loop phosphorylation of the STE20/SPS1-related proline/alanine-rich kinase (SPAK) at Thr233, which was accompanied by phosphorylation of NKCC1 at Thr203/207/212, one of which (Thr207) is responsible for cotransporter activation. Therefore, phosphorylation-induced activation of NKCC1 by osmotic shrinkage does not involve AMPK and is likely to be due to SPAK activation.

(Received 11 December 2009; accepted after revision 29 April 2010; first published online 4 May 2010)
Corresponding author M. H. Rider: de Duve Institute 75.29, Avenue Hippocrate 74, B-1200 Brussels, Belgium. Email: mark.rider@uclouvain.be

Abbreviations AICAR, 5-aminoimidazole-4-carboxamide riboside; AMPK, AMP-activated protein kinase; CaMKKβ, Ca^{2+}/calmodulin-dependent protein kinase kinase-β; GST, Glutathione-S-Transferase; NCC, Na^+–Cl^- cotransporter; NKCC1, Na^+–K^+–$2Cl^-$ cotransporter; OSR1, oxidative stress resonse protein kinase-1; PDH, pyruvate dehydrogenase; SPAK, STE20/SPS1-related proline/alanine-rich kinase; WNK, with-no-lysine (K) protein kinase.

Introduction

The Na^+–K^+–$2Cl^-$ cotransporter 1 (NKCC1) is a ubiquitously expressed electroneutral Na^+-dependent transporter involved in cell volume homeostasis and in the regulation of intracellular K^+ and Cl^- concentrations. NKCC1 is stimulated by cell shrinkage, metabolic/exercise stress, mechanical stress and ischaemia/hypoxia, and its physiology and pathophysiology in blood, brain and heart have been extensively reviewed (Pedersen *et al.* 2006). Stimulation of NKCC1 activity by osmotic shrinkage has been proposed to participate in the process of 'regulatory volume increase' (RVI) and can be inhibited by the loop diuretic drug, bumetanide. In red blood cells (RBCs), NKCC1 is activated by hyperosmolarity (Lytle, 1997) and by treatment with sodium arsenite (Flatman & Creanor, 1999*a*) or calyculin A (Lytle, 1997; Flatman & Creanor, 1999*b*). The STE20/SPS1-related proline/alanine-rich kinase (SPAK) and the homologous oxidative stress response kinase-1 (OSR1)

DOI: 10.1113/jphysiol.2009.185900

have been shown to bind to NKCC1 and its related gene product, NKCC2 (Piechotta *et al.* 2002). SPAK activates NKCC1 by phosphorylation (Dowd & Forbush, 2003) at three conserved threonine residues, Thr203, Thr207 and Thr212, in the human sequence (Vitari *et al.* 2006). Phosphorylation of Thr189 in dogfish NKCC1, equivalent to Thr207 in human NKCC1, is essential for transport activation (Flemmer *et al.* 2002). Hypertonic activation of NKCC2, which is predominantly expressed in kidney and involved in renal salt re-absorption, requires phosphorylation of all three analogous residues (Thr99, Thr104 and Thr117, rabbit sequence) for a full response (Gimenéz & Forbush, 2005). The human Na^+–Cl^- cotransporter (NCC) is also activated by phosphorylation by SPAK/OSR1 at three conserved threonine residues (Richardson *et al.* 2008). Interestingly, the SPAK and OSR1 kinases are downstream of WNK1 (with-no-lysine (K) protein kinase-1), which harbours gain-of-function mutations in Gordon's hypertension syndrome (Vitari *et al.* 2005). Phosphorylation-induced activation of SPAK and OSR1 by WNK1 occurs in the activation (T-) loop at Thr233 and Thr185, respectively (Vitari *et al.* 2005). Therefore, activation of WNK isozymes under hyperosmotic conditions leads to the activation of SPAK and OSR1, which in turn phosphorylate and activate ion cotransporters (Richardson & Alessi, 2008). Recently, AMP-activated protein kinase (AMPK) was shown to phosphorylate NKCC2 on Ser126, whose mutation to alanine reduced cotransporter activity (Fraser *et al.* 2007). Since AMPK activity was increased in kidney in response to salt intake (Fraser *et al.* 2005), phosphorylation-induced NKCC2 activation was proposed to contribute to renal salt re-absorption (Fraser *et al.* 2007).

AMPK is a highly conserved eukaryotic serine/threonine protein kinase that acts not only as a sensor of cellular energy status, but also plays a critical role in systemic energy balance (Hardie *et al.* 1998; Kahn *et al.* 2005; Witters *et al.* 2006; Hardie 2007; Steinberg & Kemp, 2009). AMPK is a heterotrimer consisting of a catalytic α subunit and two regulatory subunits, β and γ. Multiple isoforms exist giving 12 possible combinations of holoenzyme with different tissue distribution and subcellular localization. AMPK can be activated by changes in the intracellular AMP:ATP ratio, as occurs for example as a result of anoxia or other stresses, or via an increase in intracellular Ca^{2+}. LKB1 (the Peutz–Jeghers protein) and Ca^{2+}/calmodulin-dependent protein kinase kinase-β (CaMKKβ) are upstream kinases that activate AMPK by phosphorylating Thr172 in the activation loop of the catalytic α-subunits. A rise in AMP allosterically stimulates AMPK activity by binding to the γ-subunits and also prevents dephosphorylation of Thr172. Once activated, AMPK phosphorylates several metabolic targets resulting in a decrease in ATP consumption and stimulation of ATP production.

It is now becoming clear that AMPK function extends beyond metabolic control and energy homeostasis, for example to the control of cell division, cell proliferation, cell architecture, cell polarity and ion transport (Hue & Rider, 2007). Since AMPK is activated by hypertonic shock (Woods *et al.* 2003) and by arsenite treatment (Corton *et al.* 1994), both of which increase NKCC1 activity in RBCs (Lytle, 1997; Flatman & Creanor, 1999*a*), we investigated whether NKCC1 was an AMPK substrate and whether AMPK activation by erythrocyte cell shrinkage could contribute to increased ion transport.

Methods

Isolation of RBCs

Blood was drawn from healthy, consenting, human volunteers or from 8- to 14-week-old male AMPKα1-deficient mice, generated in a mixed C57BL/6 and 129Sv genetic background as described previously (Jorgensen *et al.* 2004), and their wild-type littermates. Experimental procedures were approved by the local animal welfare committee and were in accordance with the policies of the *Journal of Physiology* (Drummond, 2009). Blood was collected from animals anaesthetized with Nembutal (40–50 mg kg^{-1} administered intraperitoneally) by cardiac puncture in heparinized tubes and processed immediately. A total of about 40 mice were used and the animals were killed by interruption of circulation. Mouse or human red cells were sedimented immediately by centrifugation at 1000 *g* for 10 min at room temperature. After removal of the upper buffy coat, erythrocytes were pelleted and wash twice in phosphate-buffered saline (PBS) supplemented with 5 mM glucose. RBCs were resuspended at 50% haematocrit in Krebs–Ringer solution without bicarbonate, but buffered with 20 mM Hepes pH 7.4, and containing 11 mM glucose. The cells were stored at 4°C for use within hours of collection or stored overnight at 4°C. All incubations were carried out at 37°C and at 5% haematocrit as described in the figure legends.

Confocal microscopy

To observe erythrocyte morphology, cells were resuspended in Hepes-buffered Krebs solution with or without 0.3 M sucrose at 10^7 cells ml^{-1}. Drops (20 μl) were smeared onto glass slides and air dried for 30 min for fixation in cold methanol for 2 min. Slides were rinsed 3 times for 5 min with PBS. Images were taken in a Zeiss Axiovert 135M microscope (Carl Zeiss MicroImaging,

Oberkochen, Germany) with a water immersion ×63 magnification.

Incubation of RBCs and measurement of NKCC1 cotransporter activity

$^{86}Rb^+$ uptake was measured as described previously (Flatman & Creanor, 1999*b*). Briefly, well-agitated RBC suspensions at 5% haematocrit in a final volume of 1.5 ml were pre-incubated for 30 min prior to the addition of 5 μCi ml^{-1} of $^{86}Rb^+$ with or without 100 μM bumetanide or as described in the figure legends. At various times, 0.1 ml samples of cell suspension were added to tubes containing 0.9 ml of ice-cold PBS and 0.4 ml of di-*n*-butylphtalate. After vortexing and centrifugation (22 000 $g \times 20$ s), the supernatants and oil were aspirated off the red cell pellets. Sedimented cells were lysed in 1 ml of distilled water and proteins were precipitated with a final concentration of 2.5% (w/v) trichloroacetic acid on ice. Following centrifugation at 22 000 $g \times 10$ min, $^{86}Rb^+$ uptake was measured on aliquots of supernatant (0.9 ml) by liquid scintillation counting. Rates of $^{86}Rb^+$ uptake were expressed per mg of haemoglobin, estimated from measurements of protein (by the Lowry method, see below) *versus* haematocrit.

AMPK assay

Lysates were prepared by adding 0.5 ml of 10 mM Hepes pH 7.4, 2 mM EDTA, 2 mM sodium pyrophosphate, 20 mM NaF, 15 mM 2-mercaptoethanol, 1% (w/v) Triton X-100 to pelleted cells from 2 ml of 5% haematocrit RBC suspensions. AMPKα1-containing heterotrimeric complexes were immunoprecipitated from 750 μg of erythrocyte lysates using anti-α1-AMPK antibody (1 μg) coupled to 40 μl of Protein G-Sepharose suspension (1:1) in lysis buffer. Immunoprecipitates were washed twice in lysis buffer and twice in assay buffer (50 mM Hepes, pH 7.2, 80 mM KCl, 1 mM EDTA, 1 mM DTT, 5 mM $MgCl_2$ and 1% (v/v) glycerol). AMPK was assayed in a final volume of 50 μl of assay buffer with 0.2 mM SAMS peptide, 0.2 mM AMP, and 0.1 mm [γ-^{32}P]MgATP (specific radioactivity: 1000 cpm pmol^{-1}), at 30°C (Davies *et al.* 1989). After 10 min, 20 μl aliquots were spotted onto Whatman P81 papers for the measurement of ^{32}P incorporation (Roskoski, 1983). One unit of protein kinase activity corresponds to the incorporation of 1 nmol of phosphate into the peptide substrate per minute under the assay conditions.

Immunoblotting

Lysates were prepared as described above for AMPK assay. Extracts (15 μl) were subjected to SDS-PAGE in 7% (w/v) acrylamide gels, to avoid interference from haemglobin subunits, and electroblotted onto nitrocellulose membranes (Trans-Blot Bio-Rad, Hercules, CA, USA). The membranes were probed with primary antibodies and blocked with 5% non-fat milk for detection of immunoreactive bands by enhanced chemiluminescence with protein A-horsedish peroxidase and the SuperSignal chemiluminescence system (Pierce, Rockford, IL, USA). Band intensities were quantified by scanning films and processing image intensities with the program Image J (133 for Mac OS X).

In vitro phosphorylation

Recombinant GST (Glutathione-S-Transferase)-dogfish NKCC1(1–260) or GST-human NCC (1–100) fusion proteins (15 μg) were incubated in phosphorylation buffer (10 mM Mops, pH 7, 10 mM magnesium acetate, 0.5 mM EDTA, 0.1% (v/v) 2-mercaptoethanol) with recombinant activated bacterially expressed $\alpha1\beta1\gamma1$-AMPK (Horman *et al.* 2008; 3 mU ml^{-1}), 0.2 mM AMP and 0.1 mM [γ-^{32}P]MgATP (specific radioactivity, 300 cpm pmol^{-1}) in a final volume of 50 μl at 30°C for up to 20 min. At the indicated times, aliquots (5 μl) were removed for SDS-PAGE, Coomassie Blue staining and gel drying for quantification of ^{32}P incorporation by phosphorimaging. Protein bands in Coomassie-stained gels were quantified (Bultot *et al.* 2009) for measurements of stoichiometries of phosphorylation, taking molecular masses of 53 800 Da and 37 810 Da for the GST-NKCC1 and GST-NCC fusion proteins.

Phosphorylation site identification by mass spectrometry

The recombinant GST-dogfish NKCC1 fusion protein (10 μg) was phosphorylated *in vitro* by AMPK and [γ-^{32}P]MgATP (specific radioactivity, 1000 cpm pmol^{-1}) as described above for 1 h and precipitated with 10% (w/v) TCA for digestion with trypsin overnight at 30°C (Horman *et al.* 2006). Peptides were separated by reverse-phase narrow-bore HPLC in a linear acetonitrile gradient at a flow rate of 200 μl min^{-1} and radioactive peaks were analysed by nanoelectrospray ionization tandem mass spectrometry in a LCQ Deca XP Plus ion-trap mass spectrometer (Thermo Finnigan, San Jose, CA, USA).

Other methods

Protein concentration was estimated (Lowry *et al.* 1951) with bovine serum albumin as standard. Data are expressed as mean ± S.E.M. A Student's two-sided *t* test was used to assess the statistical significance ($P < 0.05$) of the data. All statistical analyses were performed using

GraphPad Prism version 4.00 (GraphPad Software, San Diego, CA, USA).

Antibodies and other reagents

Anti-phospho-Thr172-AMPKα antibody was from Cell Signaling Technology (Beverly, MA, USA) and T4 mouse monoclonal anti-NKCC antibody was from American Research Products, Inc. (EMELCA Bioscience, Antwerp, Belgium). Anti-α1 AMPK, anti-CaMKKβ and pyruvate dehydrogenase (PDH) antibodies were donated by Prof. D. G. Hardie (Dundee University, Scotland). Recombinant GST-dogfish NKCC1 (1–260), recombinant GST-human NCC (1–100) and anti-phospho-Thr233, anti-phospho-Ser373-SPAK, anti-total SPAK, anti-phospho-Thr203/Thr207/Thr212-NKCC1, anti-WNK and anti-OSR1 antibodies were kindly provided by Prof. D. R. Alessi (University of Dundee, Scotland). Polyclonal antibodies were raised against phosphopeptides corresponding to the sequences surrounding Ser77 and Ser242 of human NKCC1, CPLGPTPpSQSRFQV and CGEKLLRPpSLGEFHD, respectively with an N-terminal cysteine for coupling to keyhole limpet haemocyanin and immunization in sheep (Sugden *et al.* 1999). Sera were first bound to columns containing the same immobilized peptides that had been used for immunization. The phospho-specific antibodies were eluted (Sugden *et al.* 1999) then passed through columns containing immobilized dephosphopeptides. Phospho-specific antibodies were tested for immunoreactivity by ELISA with the immunizing antigen and for specificity by immunoblotting. Anti-sheep, anti-mouse and anti-rabbit IgG conjugated to peroxidase were purchased from Sigma (St Louis, MO), Santa Cruz Biotechnology (Santa Cruz, CA, USA) and GE Healthcare (Little Chalfont, UK), respectively. A769662 was kindly given by Dr A. Balandran (AstraZeneca, Mölndal, Sweden). STO-609 was from Calbiochem (La Jolla, CA, USA) and bumetanide was from Biomol Research Laboratories Inc. (Plymouth, PA, USA). Radioactive $^{86}Rb^{+}$ (37.0 GBq g^{-1}) and [γ-^{32}P]ATP (111 TBq mmol^{-1}) were from Perkin-Elmer (Billerica, MA, USA). Recombinant bacterially expressed $\alpha1\beta1\gamma1$-AMPK heterotrimers were kindly provided by Dr D. Neumann (ETH Zurich, Switzerland) and activated as described (Horman *et al.* 2008).

Results

In vitro phosphorylation of NKCC1 by AMPK and phosphorylation site identification

A recombinant N-terminal fragment (residues 1–260 corresponding to the intracellular cytosolic domain) of dogfish NKCC1 fused to GST was phosphorylated *in vitro* from [γ-^{32}P]MgATP and recombinant activated $\alpha1\beta1\gamma1$-AMPK heterotrimers (Fig. 1*A*). Phosphorylation was time dependent reaching a maximal stoichiometry of about 0.8 mole of phosphate incorporated/mole of GST-NKCC1 (1–260). However, with a second batch of GST-NKCC1 (1–260), maximal phosphorylation by AMPK reached a stoichiometry of 1.79 ± 0.11 mol mol^{-1} ($n = 4$, results not shown), suggesting that two sites could be phosphorylated. The differences in stoichiometry of phosphorylation by AMPK might have been due to differences in the proportion of recombinant GST-NKCC1 protein present in the proper conformation for phosphorylation by AMPK in the two preparations. A recombinant N-terminal fragment (residues 1–100) of the related human NCC transporter was a poor AMPK substrate, whose maximal stoichiometry of phosphorylation was only 0.07 mol mol^{-1} (Fig. 1*A*). After maximal phosphorylation of the first GST-dogfish NKCC1 preparation by AMPK and [γ-^{32}P]MgATP, the protein was precipitated, digested with trypsin and the peptides separated by HPLC. The major radioactive peaks (Fig. 1*B*) were analysed by mass spectrometry. In peaks I and II, Ser214 was identified as the phosphorylation site in the phosphorylated peptides LIRP**S**LAELHDELDK and LIRP**S**LAELHDELDKEPFEDGYVNGEESSPAEEA (corresponding to a non-specific tryptic peptide with one missed cleavage), respectively, of the dogfish NKCC1 sequence. Ser214 of dogfish NKCC1 corresponds to Ser242 of the human protein and to the AMPK site previously identified in rabbit renal NKCC2 (Ser126) based on a sequence alignment (Fig. 1*C*). The phosphorylation site in peak III (Fig. 1*B*) was identified as Ser38 in the phosphorylated tryptic peptide (SQSGPEPGAGQQEPPPPATPLRPVA**S**QSR) of the dogfish NKCC1 sequence after re-digestion of fractions 43 + 44 by chymotrypsin. This site corresponds to Ser77 of human NKCC1 (Fig. 1*C*). It is not conserved in rabbit NKCC2 and is not present in human NCC. None of the AMPK sites identified in NKCC1 correspond to the SPAK/OSR1 sites (Thr203/207/212) implicated in human NKCC1 activation.

Polyclonal sheep antibodies were raised against phosphorylated peptides corresponding to the sequences surrounding Ser77 and Ser242 of human NKCC1. The specificity of the antibodies was verified by immunoblotting purified GST-dogfish NKCC1 (1–260), phosphorylated with or without activated AMPK and non-radioactive MgATP (Supplemental Fig. S1A).

Effect of A769662 on AMPK activation, NKCC1 phosphorylation and $^{86}Rb^{+}$ uptake in human RBCs

Since treatment of erythrocytes with 5-aminoimidazole-4-carboxamide riboside (AICAR, which is converted in

cells to the AMP analogue, ZMP) does not lead to AMPK activation in RBCs (results not shown and B. Viollet, personal communication), human erythrocytes were incubated with the recently discovered small-molecule, non-nucleotide, thienopyridone A769662 AMPK activator (Cool *et al.* 2006). Incubation with 20 μM A769662 led to a time-dependent increase in AMPK activity reaching a plateau of about 2-fold after 20 min (data not shown) and after 30 min, a significant increase in AMPK Thr172 phosphorylation of about 50% (Fig. 2*A*) accompanied AMPK activation. Therefore, the phosphorylation state of the two new AMPK sites in NKCC1 was investigated using the phospho-specific antibodies that had been generated in sheep. After 30 min of incubation with A769662, no change in Ser77 NKCC1 phosphorylation in response to A769662 treatment occurred, whereas for the Ser242 NKCC1 site there was a significant 50% increase in phosphorylation, with no change in phosphorylation state of the conserved Thr203/207/212 NKCC1 sites (Fig. 2*B*), of which Thr207 phosphorylation is required for NKCC1 cotransporter activation. Total $^{86}Rb^{+}$ uptake was likewise unaffected (Fig. 2*C*), suggesting that AMPK activation by A769662 is not linked to NKCC1 activation.

Hyperosmolarity induces shrinkage, AMPK activation and stimulation of bumetanide-sensitive $^{86}Rb^{+}$ uptake in human RBCs

Incubation of human erythrocytes to induce hyperosmotic shock with 0.3 M sucrose (added to the Krebs–Ringer solution) led to cell shrinkage as observed

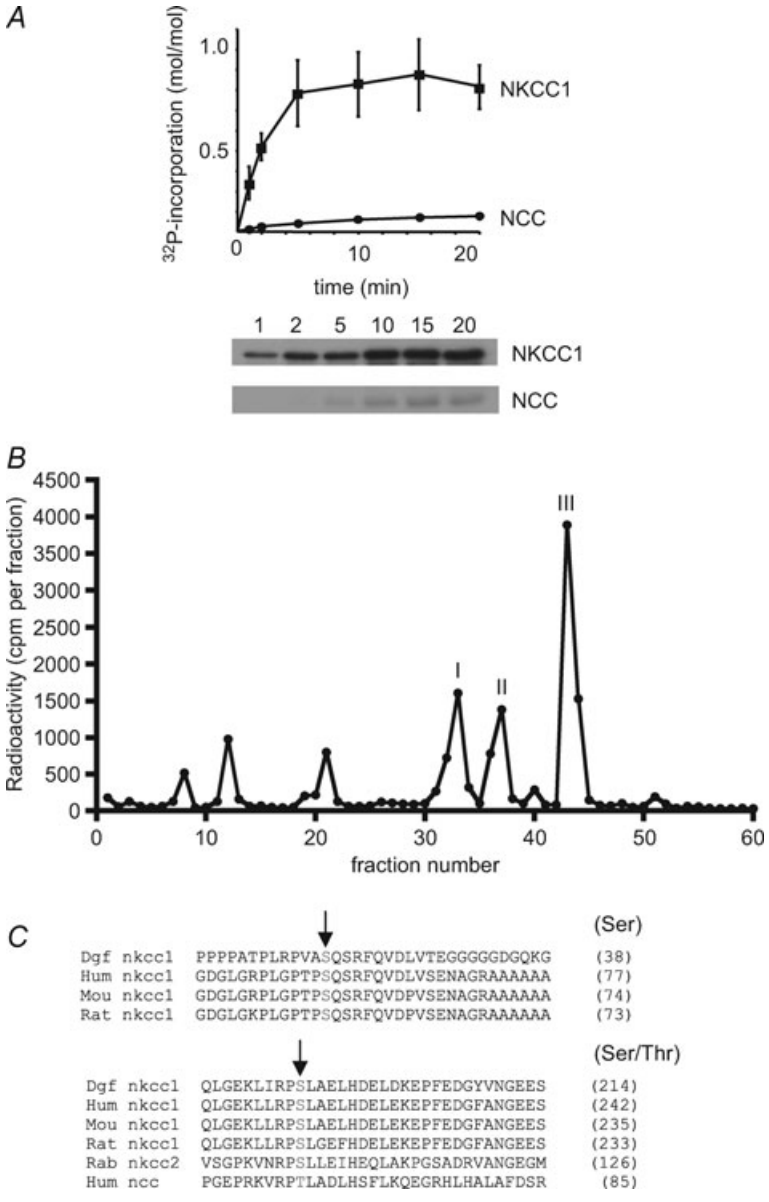

Figure 1. Phosphorylation of NKCC1 by AMPK and identification of the sites
A, recombinant GST-dogfish NKCC1 and GST-human NCC were phosphorylated *in vitro* with AMPK and [γ-^{32}P]MgATP. At the indicated times, aliquots were removed for SDS-PAGE and phosphorimaging for the measurement of ^{32}P incorporation. The results are the means ± S.E.M. of three separate experiments and representative autoradiograms are shown below. *B*, after maximal *in vitro* phosphorylation by AMPK, GST-dogfish NKCC1 was precipitated and digested with trypsin. Peptides were separated by reverse-phase narrow-bore HPLC in an acetonitrile gradient and fractions were counted by Cerenkov radiation. Phosphorylation sites in the three radiolabelled peaks were identified by mass spectrometry. *C*, an alignment of N-terminal domain sequences surrounding the AMPK sites of dogfish NKCC1 with human, mouse and rat, as well as with sequences of rabbit NKCC2 and human NCC is shown. AMPK phosphorylation sites in dogfish NKCC1 are indicated by arrows and numbers between brackets refer to the residues corresponding to dogfish Ser38 and Ser214 in the different species.

by fixation and confocal microscopy (not shown). Under these conditions, AMPK Thr172 phosphorylation increased rapidly becoming significant after 1 min and reaching a maximum at 30 min (Fig. 3*A*). Accordingly, AMPK activity increased up to 2-fold after 30 min of incubation under hyperosmotic conditions compared to basal activity (Fig. 3*B*). We then tested whether cell shrinkage would increase NKCC1 activity as measured by bumetanide-sensitive $^{86}Rb^+$ uptake in human erythrocytes. RBCs were preincubated for 30 min with sucrose to fully activate AMPK with or without the NKCC1 inhibitor bumetanide. $^{86}Rb^+$ tracer was then added and the rate of ion uptake was measured over 60 min (Fig. 3*C*). Cell shrinkage with 0.3 M sucrose increased the initial rate of total $^{86}Rb^+$ uptake about 2-fold compared with the controls (Fig. 3*D*) and the hyperosmolarity-induced increase in $^{86}Rb^+$ uptake was inhibited by about 60% at 60 min by incubation with bumetanide (Fig. 3*C*). Moreover, the stimulation of ion uptake by hyperosmolarity was completely abrogated by bumetanide addition (Fig. 3*C* and *D*). Therefore in human erythrocytes, cell shrinkage induced by sucrose addition led to both AMPK activation and an increase in NKCC1 activity.

AMPKα1 deletion in mice has no effect on hyperosmolarity-induced NKCC1 activation

Since the major AMPK catalytic subunit isoform in RBCs is α1-AMPK (Föller *et al.* 2009 and our data not shown), we took advantage of a mouse model in which the AMPKα1 subunit isoform had been deleted to explore the potential link between AMPK activation and the stimulation of NKCC1 activity during hyperosmotic stress. The cell shrinkage-induced increase in $^{86}Rb^+$ uptake was compared in erythrocytes from wild-type

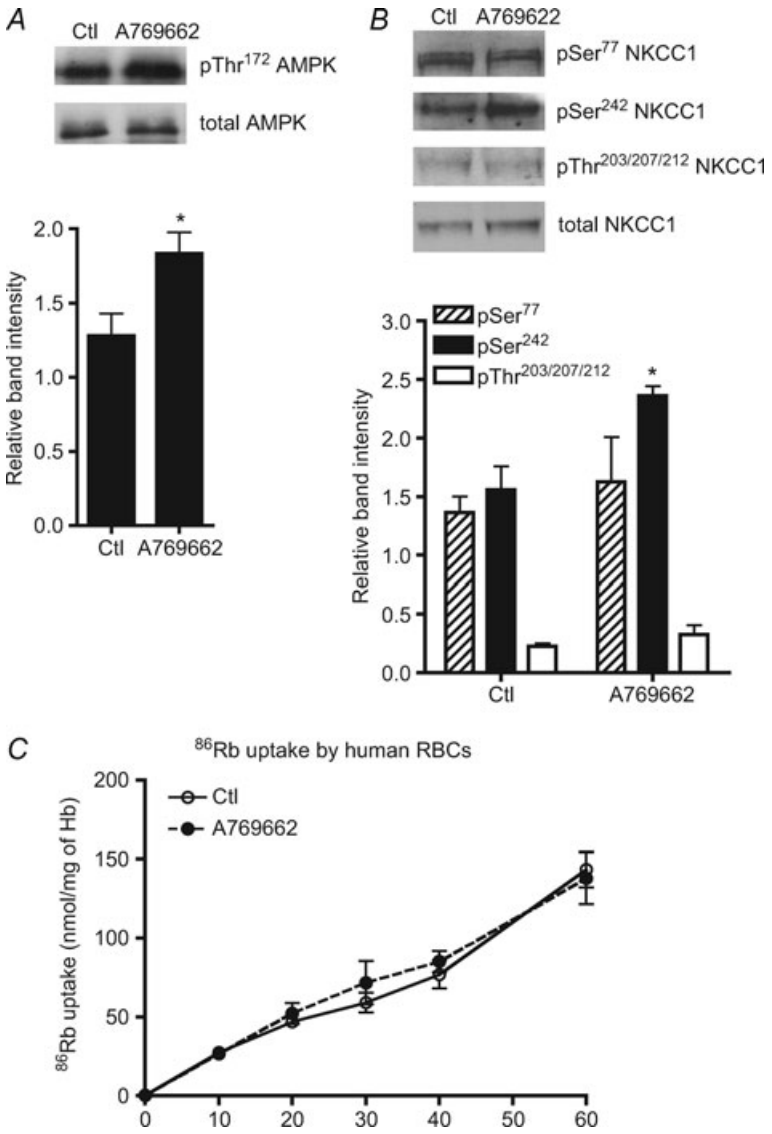

Figure 2. Effect of A769662 treatment on AMPK activation, SPAK and NKCC1 phosphorylation and $^{86}Rb^+$ uptake in human RBCs
Washed human erythrocytes were incubated with 20 μM A769662 for 30 min and extracts were prepared for immunoblotting as described in Methods. *A*, upper panel, a representative immunoblot of α-AMPK Thr172 phosphorylation *versus* total α1-AMPK. *B*, upper panel, representative immunoblots of NKCC1 Ser77, Ser242 and Thr203/207/212 phosphorylation *versus* total NKCC1. Densitometric scanning ratios of band intensities obtained with the anti-phospho antibodies relative to those obtained for the loading controls are shown in the lower panels and the results are the means ± S.E.M. of three independent experiments. *Significant difference ($P < 0.05$, paired *t* test) with respect to the controls. *C*, washed RBCs were pre-incubated at 5% haematocrit and 37°C in Hepes-buffered Krebs medium containing 11 mM glucose, without (○) or with (●) 20 μM A-769662. After 20 min, tracer $^{86}Rb^+$ (5 μCi ml^{-1}) was added to the suspension at $t = 0$ and uptake was followed at the indicated times over 60 min. The results are the means ± S.E.M. of four independent experiments.

(Fig. 4*A*) and AMPKα1-deficient mice (Fig. 4*B*). No effect of AMPKα1 deletion on the rate of basal $^{86}Rb^+$ uptake, the hyperosmolarity-induced increase in total $^{86}Rb^+$ uptake or the bumetanide-sensitive increase in uptake by hyperosmolarity was seen (Fig. 4*C*).

Effect of STO-609 on hyperosmolarity-induced AMPK activation and $^{86}Rb^+$ uptake in mouse RBCs

When mouse erythrocytes were incubated with the STO-609 selective CaMKKβ inhibitor, AMPK activation by 0.3 M sucrose was abrogated (Fig. 5*A*), suggesting that hyperosmolarity-induced AMPK activation involves a rise in intracellular Ca^{2+} and phosphorylation of the α-subunit Thr172 residue by CaMKKβ. Both mouse and human RBCs were found to contain both CaMKKβ and LKB1 as detected by immunoblotting of full lysates (Fig. S1B). Although incubation with STO-609 abrogated AMPK activation by cell shrinkage, it did not significantly reduce the hyperosmolarity-induced increase in total $^{86}Rb^+$ uptake (Fig. 5*B*) and an increase in bumetanide-sensitive uptake was still seen in the presence of sucrose and

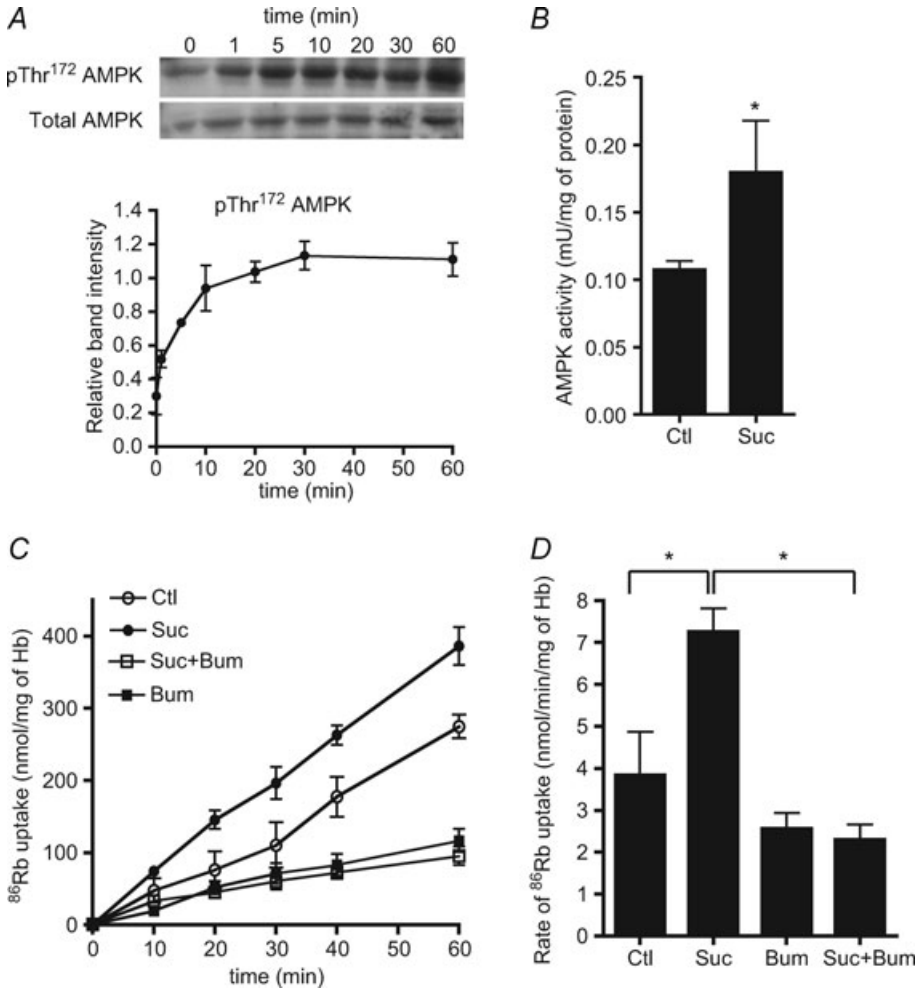

Figure 3. Effects of hyperosmolarity on AMPK activity and bumetanide-sensitive $^{86}Rb^+$ uptake in human RBCs

Washed human erythrocytes were incubated with 0.3 M sucrose for the indicated times and extracts were analysed by immunoblotting. *A*, upper panel, a representative immunoblot of α-AMPK Thr172 phosphorylation *versus* total α1-AMPK. Densitometric scanning ratios of phospho/total AMPK are shown in the lower panel and the results are the means ± S.E.M. of three independent experiments. *B*, extracts from erythrocytes incubated with 0.3 M sucrose for 30 min were immunoprecipitated with anti-AMPK α1-subunit antibody for AMPK assay. The results are the means ± S.E.M. of three independent experiments. *Significant difference ($P < 0.05$, paired *t* test) with respect to the controls. *C*, washed human RBCs were incubated at 5% haematocrit and 37°C in Hepes-buffered Krebs medium containing 11 mM glucose, without (○) or with (●) 0.3 M sucrose or with 100 μM bumetanide (□) or sucrose + bumetanide (■). After 30 min, tracer $^{86}Rb^+$ (5 μCi ml^{-1}) was added to the suspension at $t = 0$ and uptake was followed at the indicated times. *D*, initial influx rates (calculated over 60 min) are the means ± S.E.M. of five independent experiments. *Significant difference ($P < 0.05$, paired *t* test).

STO-609. Therefore, together with results obtained in α1-AMPK deficient mice, the findings suggest that AMPK activation and stimulation of NKCC1 activity by hyperosmolarity are parallel events that are not causatively linked.

Effects of A769662 and hyperosmolarity on SPAK/NKCC1phosphorylation and $^{86}Rb^+$ uptake in mouse RBCs

Mouse and human RBCs were found to contain WNK1 and OSR1, as detected by immunoblotting, as well as CaMKKβ and LKB1 (Fig. S1B). To assess possible contamination from non-RBCs, we immunoblotted extracts from washed erythrocytes using an antibody raised against human pyruvate dehyrogenase (PDH), a mitochondrial enzyme marker, to indicate contamination by white cells. No signal could be detected in red cell lysates, whereas a strong band was detected in hepatocyte extracts as positive control (Fig. S1C). Therefore, contamination of our preparations by non-red cells was minimal.

Incubation of human RBCs with 0.3 M sucrose led to a time-dependent increase in SPAK activation loop Thr233 phosphorylation, along with the second site on SPAK phosphorylated by WNK1, namely Ser373, which is not required for activation (Fig. S2A). Moreover, SPAK activation by osmotic shrinkage correlated closely with NKCC1 phosphorylation on the three conserved Thr residues (Fig. S2B). Therefore, mouse RBCs were incubated for different times with A769662 and sucrose to further investigate the possible correlation between NKCC1 phosphorylation and stimulation of bumetanide-sensitive $^{86}Rb^+$ uptake. Incubation with A769662 or sucrose led to AMPK Thr172 phosphorylation, as observed in human RBCs (Figs 2*A* and 3*A*), and AMPK activation by A769662

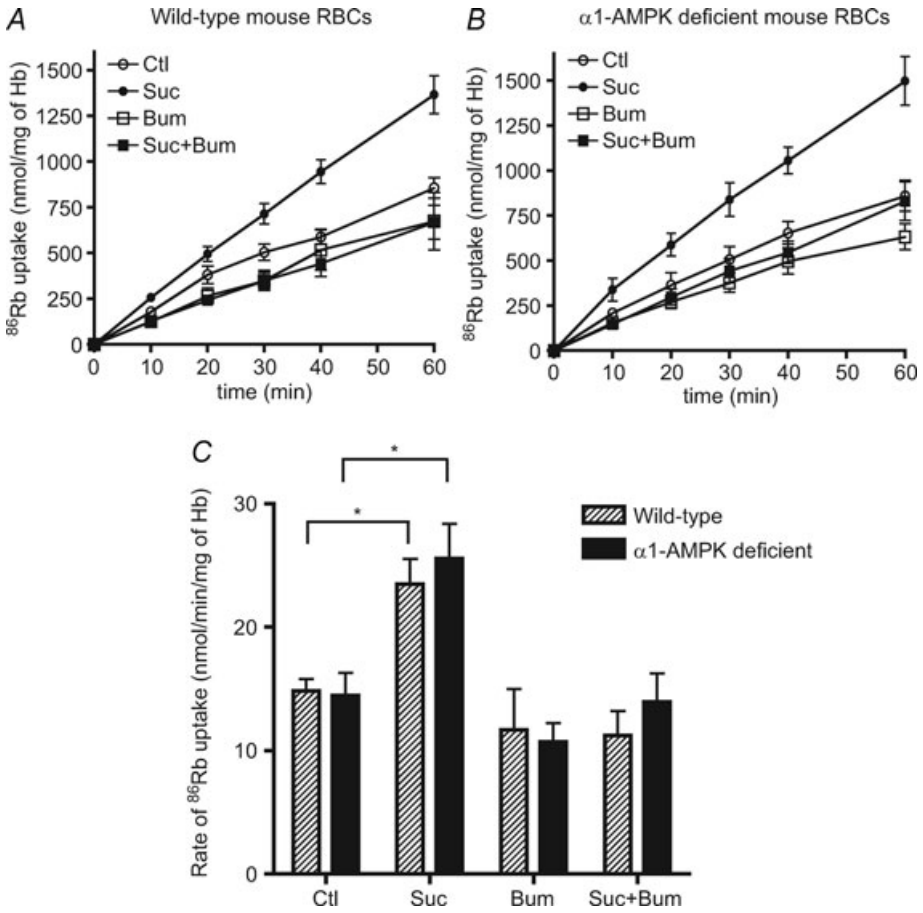

Figure 4. Effect of hyperosmolarity induced by sucrose treatment on $^{86}Rb^+$ uptake in erythrocytes from wild-type and AMPKα1-deficient mice

Washed erythrocytes from wild-type and AMPKα1-deficient mice were incubated with and without 0.3 M sucrose, with and without 100 μM bumetanide for $^{86}Rb^+$ uptake measurements at the indicated times. The results are the means ± S.E.M. of five independent experiments. *C*, initial influx rates of $^{86}Rb^+$ uptake were measured in the presence and absence of 100 μM bumetanide (see legend to Fig. 3). *Significant difference ($P < 0.05$, paired *t* test).

treatment was greater at 60 min of incubation than at 5 min (Fig. 6*A*). Incubation with A769662 had no effect on SPAK Thr233, SPAK Ser373 (Fig. 6*B*) and NKCC1 Thr203/207/212 phosphorylation (Fig. 7*A*) and was without effect on bumetanide-sensitive $^{86}Rb^+$ uptake (Fig. 7*B*) either at 5 or at 60 min of incubation. In response to hyperosmolarity, SPAK Thr233 activation loop phosphorylation was maximal at 5 and 60 min of incubation (Fig. 6*B*) whereas the level of NKCC1 Thr203/207/212 phosphorylation was greater at 60 min than at 5 min (Fig. 7*A*). Bumetanide-sensitive $^{86}Rb^+$ uptake was slightly greater at 60 min than at 5 min of incubation with sucrose (Fig. 7*B*) and so the extent of NKCC1 phosphorylation did not directly correlate with NKCC1 activation by hyperosmolarity in mouse RBCs and other factors are likely involved.

Discussion

At the outset of this work, little was known about the AMPK and WNK/SPAK systems in RBCs and the molecular mechanism by which cell shrinkage activates NKCC1 in erythrocytes had not been clarified. Our aim was to investigate the mechanisms by which hyperosmolarity increases NKCC1 cotransporter activity and particularly whether AMPK activation could be implicated. We show that similar to NKCC2, NKCC1 can be phosphorylated by AMPK. Phosphorylation of NKCC1 occurred at Ser38 and Ser214 (dogfish sequence) corresponding to Ser77 and Ser242 in human NKCC1. The AMPK phosphorylation recognition motif is ϕ(Xβ)XXS/TXXXϕ where ϕ is a hydrophobic residue (M, V, L, I or F), β is a basic residue (R, K or H) and the parentheses indicate that the order of residues at the P-4 and P-3 positions is not critical (Dale *et al.* 1995). The sequence surrounding Ser242 of human NKCC1 loosely fits the AMPK consensus, with an Arg residue at the P-2 rather than P-3 position. The corresponding residue in human NCC is Thr85 and flanked by Arg residues at P-2 and P-5 plus a Lys at P-4, explaining its poor rate of phosphorylation by AMPK. Ser38 of dogfish NKCC1 lies in a perfect context for phosphorylation by AMPK, which is not as favourable in the mammalian sequences due to the absence of a basic residue. However, the corresponding Ser77 residue of human NKCC1 was found to be phosphorylated in a phosphoproteomics study of HeLa cells subjected to cell cycle arrest (Dephoure *et al.* 2008).

Although the increase in $^{86}Rb^+$ uptake by cell shrinkage in RBCs was associated with AMPK activation, phosphorylation of NKCC1 by AMPK is unlikely to be involved for the following reasons: (i) incubation of RBCs with A769662 to activate AMPK did not increase $^{86}Rb^+$ uptake from either human or mouse cells, although phosphorylation at Ser242 of NKCC1 was increased in human erythrocytes; (ii) AMPKα1 deletion in mouse RBCs had no effect on the increase in rate of bumetanide-sensitive $^{86}Rb^+$ uptake by hyperosmolarity; (iii) STO-609 treatment of mouse RBCs

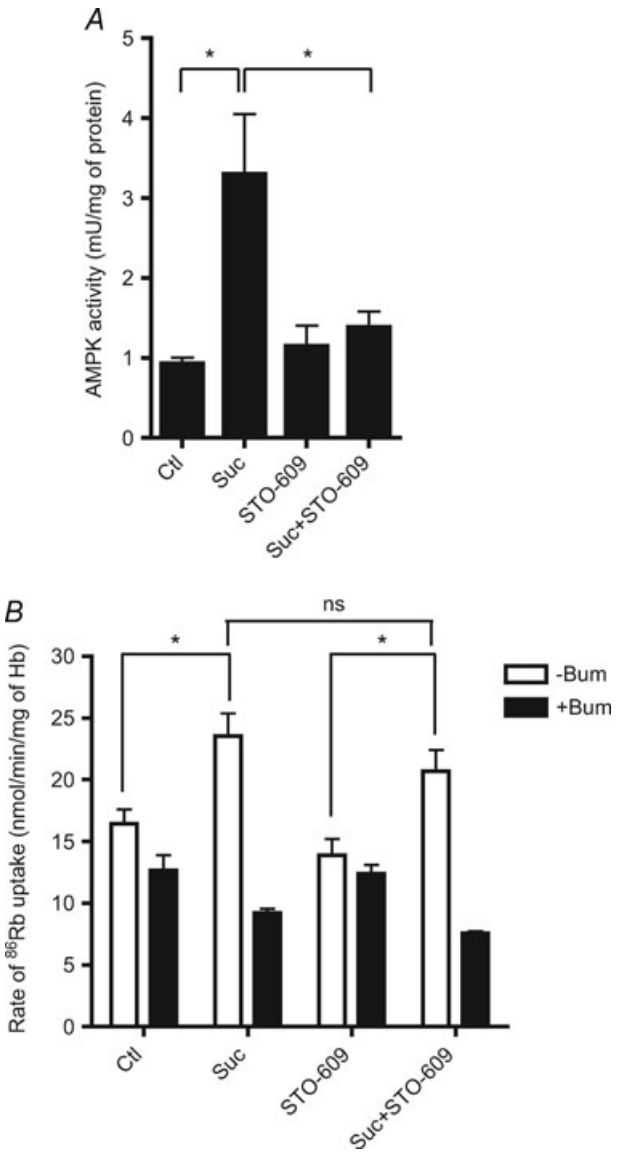

Figure 5. Effect of the STO-609 CaMKKβ inhibitor on hyperosmolarity-induced AMPK activation and $^{86}Rb^+$ uptake in mouse RBCs

Washed mouse erythrocytes were incubated at 5% haematocrit and 37°C in Hepes-buffered Krebs medium containing 11 mM glucose, with or without 10 μM STO-609 and with or without 0.3 M sucrose for 30 min. *A*, extracts were immunoprecipated with anti-AMPK α1-subunit antibody for AMPK assay. The results are the means ± S.E.M. of three independent experiments. *B*, after 30 min, initial rates of $^{86}Rb^+$ uptake were calculated from measurements made at 10 and 30 min in the presence and absence of 100 μM bumetanide. The results are the means ± S.E.M. of six independent experiments. *Significant difference ($P < 0.05$, paired *t* test).

abrogated AMPK activation by hyperosmolarity but did not significantly reduce bumetanide-sensitive $^{86}Rb^{+}$ uptake. Although human RBCs clearly express CaMKKβ (Fig. S1B), it remains to be seen whether STO-609 would block hyperosmolarity-induced AMPK activation, as observed in mouse RBCs. AMPK activation by A769662 involves allosteric stimulation of activity and inhibition of dephosphorylation by protein phosphatases, which increases the extent of its activation loop Thr172 phosphorylation (Sanders *et al.* 2007). Extracts were routinely prepared with direct lysis without washing the cells and AMPK activation was assessed after immunoprecipitation (Fig. S2B), which washes away the AMPK activator and so activation could not have occurred after lysis. AMPK activation was also assessed by immunoblotting (Fig. 2*A*), clearly showing that Thr172 phosphorylation was increased and that the AMPK activator was effective in the intact cells. Therefore, lack

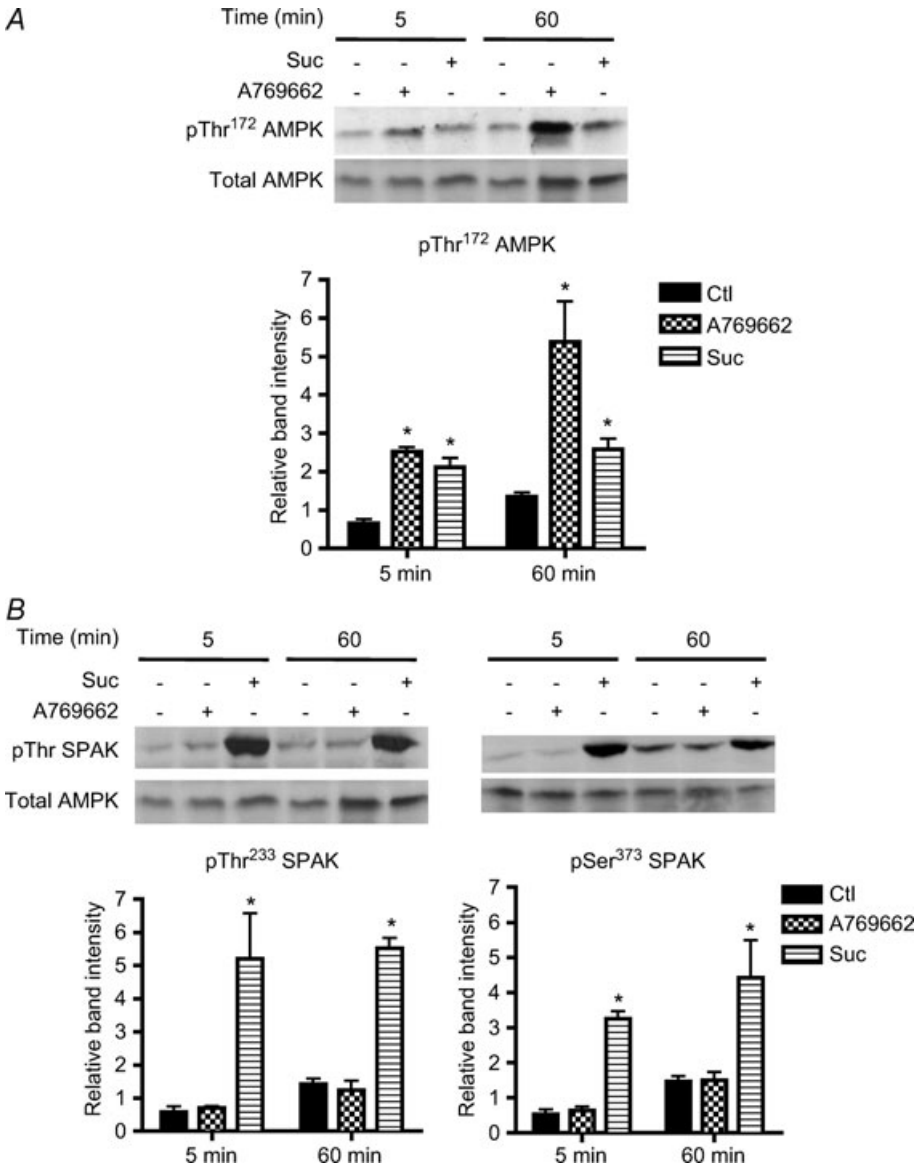

Figure 6. Effect of hyperosmolarity and A769662 treatment on AMPK and SPAK phosphorylation in mouse RBCs

Washed mouse erythrocytes were incubated at 5% haematocrit and 37°C in Hepes-buffered Krebs medium containing 11 mM glucose, with or without 20 μM A769662 and with or without 0.3 M sucrose for 5 or 60 min. *A*, upper panel, a representative immunoblot of α-AMPK Thr172 phosphorylation *versus* total α1-AMPK. *B*, upper panels, representative immunoblots of SPAK Thr233 and Ser373 phosphorylation *versus* total AMPK as a loading control. Lower panels, densitometric scanning ratios of band intensities obtained with the anti-phospho antibodies relative to those obtained for the loading controls; the results are the means ± S.E.M. of three independent experiments. *Significant difference ($P < 0.05$, paired *t* test) with respect to the controls.

of permeation of A769662 could not explain the lack of effect on ion transport. Moreover, in freshly isolated rat cardiomyoctes treated with A769662 or oligomycin and in rat hepatocytes incubated with A769662 or AICA riboside to activate AMPK, there was no stimulation of $^{86}Rb^{+}$ uptake (Fig. S3).

Surprisingly, incubation of human RBCs with sodium arsenite did not increase $^{86}Rb^{+}$ uptake, contrary to its stimulatory effect in ferret red cells (Flatman & Creanor 1999*a*), and did not lead to AMPK activation (data not shown) as reported in rat hepatocytes (Corton *et al.* 1994). The lack of effect of arsenite in human compared with ferret RBCs could imply that arsenite treatment does not lead to activation of the signalling pathway responsible for NKCC1 activation in human cells or that this toxic compound is 'neutralized' in human but not ferret erythrocytes. Also, there is variation in the responses of RBCs from different species due to differences in the transporters present, the regulatory apparatus, and expression of membrane proteins and their association with glycolytic enzymes (Pasini *et al.* 2010). Indeed, AMPK activities and rates of $^{86}Rb^{+}$ uptake in human erythrocytes (Fig. 3) were somewhat less than in mouse RBCs (Fig. 5). Also, the responses of RBC subpopulations may be different,

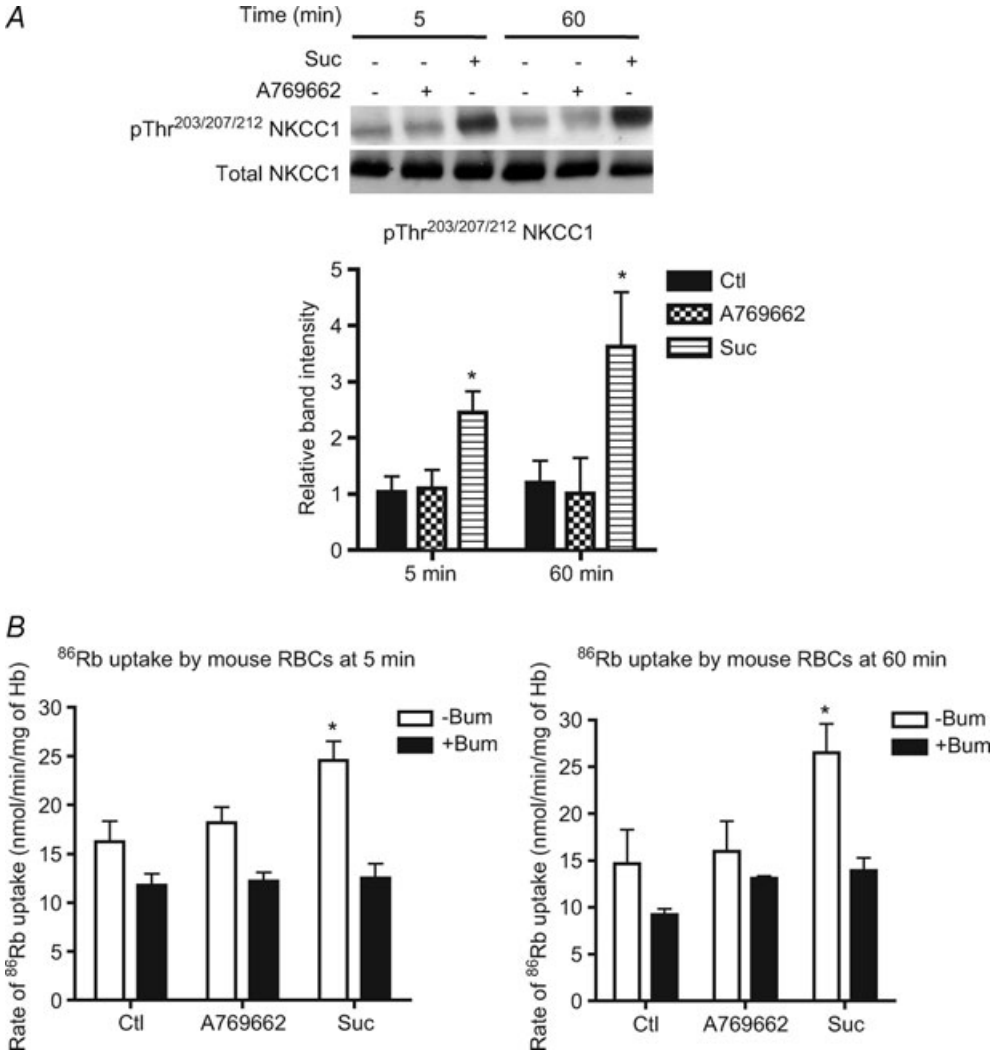

Figure 7. Effect of hyperosmolarity and A769662 treatment on NKCC1 phosphorylation and bumetanide-sensitive $^{86}Rb^{+}$ uptake in mouse RBCs

Washed mouse erythrocytes were incubated at 5% haematocrit and 37°C in Hepes-buffered Krebs medium containing 11 mM glucose, with or without 20 μM A769662 and with or without 0.3 M sucrose for 5 or 60 min. *A*, upper panel, a representative immunoblot of NKCC1 Thr203/207/212 phosphorylation *versus* total NKCC1 Densitometric scanning ratios of band intensities obtained with the anti-phospho antibodies relative to those obtained for the loading controls are shown in the lower panel. *B*, initial rates of $^{86}Rb^{+}$ uptake were measured in the presence and absence of 100 μM bumetanide (see legend to Fig. 3). The results are the means ± S.E.M. of three independent experiments. *Significant difference ($P < 0.05$, paired *t* test) with respect to the controls.

for example in ageing erythrocytes enzyme activities can decrease as the cells become smaller.

Osmotic shrinkage led to SPAK activation loop phosphorylation in mouse and human RBCs, which was accompanied by phosphorylation of the three conserved Thr residues of NKCC1. Therefore, activation of the WNK1/SPAK pathway by hyperosmolarity could explain the increase in $^{86}Rb^+$ uptake. One effect of adding 0.3 M sucrose to red cells is that the intracellular Cl^- (as well as Na^+ and K^+) concentration would be increased by shrinkage. The increase in cellular Cl^- concentration should in turn shift the Donnan equilibrium between intracellular Cl^- and OH^- ions and alkalinize the cells slightly. To the best of our knowledge, there is no information in the literature on the pH–activity profiles of WNK or SPAK. It is possible that cytosolic alkalinization might reinforce or oppose the effects of cell shrinkage on the activities of the WNK1/SPAK kinases involved in NKCC1 activation.

In conclusion, increased $^{86}Rb^+$ uptake by osmotic shrinkage seems to be due to activation of the WNK1/SPAK, rather than the AMPK pathway. AMPK was activated by hyperosmolarity in RBCs, probably secondary to a rise in Ca^{2+} via CaMKKβ. Although NKCC1 phosphorylation by AMPK does not appear to directly control cotransporter activity, the AMPK Ser77 site was detected as being phosphorylated *in vivo* in a phosphoproteomics study (Dephoure *et al.* 2008) and treatment of human RBCs with A769662 led to an increase in phosphorylation of Ser242, the second AMPK site we identified. Interestingly, two-dimensional phosphopeptide mapping of RBCs indicated that NKCC1 acquires five phosphates going from an inactive state to an active state in shrunken cells (Lytle, 1997). However, we were unable to see changes in Ser77 or Ser242 phosphorylation of NKCC1 during hyperosmolarity. Phosphorylation of Ser77/242 by AMPK could affect NKCC1 function other than its ion transport activity (Fig. 8). NKCC1 has many interacting partners including PP1, p38 MAPK, MLCK, PKCδ and SPAK, and is also regulated by the F-actin cytoskeleton (Hoffmann *et al.* 2007, 2009).

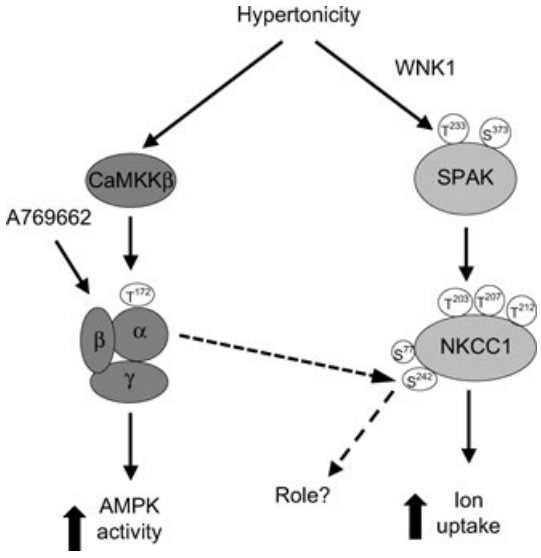

Figure 8. Activation of the WNK1/SPAK and CaMKKβ/AMPK pathways by osmotic shrinkage in RBCs
Cell shrinkage by sucrose treatment in RBCs leads to activation of α1-AMPK and SPAK via the CaMKKβ and WNK1 pathways, respectively. SPAK activation correlates with NKCC1 Thr203/207/212 phosphorylation and is likely to be responsible for its activation and increased $^{86}Rb^+$ uptake induced by hyperosmolarity. AMPK activation by hyperosmolarity does not affect NKCC1 activity. Treatment with A-769662 activates AMPK in RBCs and increases Ser242 NKCC1 phosphorylation, whose function is at present unknown. The proposed scheme is based on the present data.

References

Bultot L, Horman S, Neumann D, Walsh MP, Hue L & Rider MH (2009). Myosin light chains are not a physiological substrate of AMPK in the control of cell structure changes. *FEBS Lett* **583**, 25–28.

Cool B, Zinker B, Chiou W, Kifle L, Cao N, Perham M, Dickinson R, Adler A, Gagne G, Iyengar R, Zhao G, Marsh K, Kym P, Jung P, Camp HS & Frevert E (2006). Identification and characterization of a small molecule AMPK activator that treats key components of type 2 diabetes and the metabolic syndrome. *Cell Metab* **3**, 403–416.

Corton JM, Gillespie JG & Hardie DG (1994). Role of the AMP-activated protein kinase in the cellular stress response. *Curr Biol* **4**, 315–324.

Dale S, Wilson WA, Edelman AM & Hardie DG (1995). Similar substrate recognition motifs for mammalian AMP-activated protein kinase, higher plant HMG-CoA reductase kinase-A, yeast SNF1, and mammalian calmodulin-dependent protein kinase I. *FEBS Lett* **361**, 191–195.

Davies SP, Carling D & Hardie DG (1989). Tissue distribution of the AMP-activated protein kinase, and lack of activation by cyclic-AMP-dependent protein kinase, studied using a specific and sensitive peptide assay. *Eur J Biochem* **186**, 123–128.

Dephoure N, Zhou C, Villén J, Beausoleil SA, Bakalarski CE, Elledge SJ & Gygi SP (2008). A quantitative atlas of mitotic phosphorylation. *Proc Natl Acad Sci U S A* **105**, 10762–10767.

Dowd BF & Forbush B (2003). PASK (proline-alanine-rich STE20-related kinase), a regulatory kinase of the Na-K-Cl cotransporter (NKCC1). *J Biol Chem* **278**, 27347–27353.

Drummond GB (2009). Reporting ethical matter in *The Journal of Physiology*: standards and advice. *J Physiol* **587**, 713–719.

Flatman PW & Creanor J (1999*a*). Regulation of Na^+-K^+-$2Cl^-$ cotransport by protein phosphorylation in ferret erythrocytes. *J Physiol* **517**, 699–708.

Flatman PW & Creanor J (1999*b*). Stimulation of Na^+-K^+-$2Cl^-$ cotransport by arsenite in ferret erythrocytes. *J Physiol* **519**, 143–152.

Flemmer AW, Gimenez I, Dowd BF, Darman RB & Forbush B (2002). Activation of the Na-K-Cl cotransporter NKCC1 detected with a phospho-specific antibody. *J Biol Chem* **277**, 37551–37558.

Föller M, Sopjani M, Koka S, Gu S, Mahmud H, Wang K, Floride E, Schleicher E, Schulz E, Münzel T & Lang F (2009). Regulation of erythrocyte survival by AMP-activated protein kinase. *FASEB J* **23**, 1072–1080.

Fraser SA, Gimenez I, Cook N, Jennings I, Katerelos M, Katsis F, Levidiotis V, Kemp BE & Power DA (2007). Regulation of the renal-specific Na^+-K^+-$2Cl^-$ co-transporter NKCC2 by AMP-activated protein kinase (AMPK). *Biochem J* **405**, 85–93.

Fraser S, Mount P, Hill R, Levidiotis V, Katsis F, Stapleton D, Kemp BE & Power DA (2005). Regulation of the energy sensor AMP-activated protein kinase in the kidney by dietary salt intake and osmolality. *Am J Physiol Renal Physiol* **288**, 578–586.

Giménez I & Forbush B (2005). Regulatory phosphorylation sites in the NH_2 terminus of the renal Na-K-Cl cotransporter (NKCC2). *Am J Physiol Renal Physiol* **289**, 1341–1345.

Hardie DG, Carling D & Carlson M (1998). The AMP-activated/SNF1 protein kinase subfamily: metabolic sensors of the eukaryotic cell? *Annu Rev Biochem* **67**, 821–855.

Hardie DG (2007). AMP-activated/SNF1 protein kinases: conserved guardians of cellular energy. *Nat Rev Mol Cell Biol* **8**, 774–785.

Hoffmann EK, Schettino T & Marshall WS (2007). The role of volume-sensitive ion transport systems in regulation of epithelial transport. *Comp Biochem Physiol A Mol Integr Physiol* **148**, 29–43.

Hoffmann EK, Lambert IH, Pedersen SF (2009). Physiology of cell volume regulation in vertebrates. *Physiol Rev* **89**, 193–277.

Horman S, Vertommen D, Heath R, Neumann D, Mouton V, Woods A, Schlattner U, Wallimann T, Carling D, Hue L & Rider MH (2006). Insulin antagonizes ischemia-induced Thr172 phosphorylation of AMP-activated protein kinase α-subunits in heart via hierarchical phosphorylation of Ser485/491. *J Biol Chem* **281**, 5335–5340.

Horman S, Morel N, Vertommen D, Hussain N, Neumann D, Beauloye C, El Najjar N, Forcet C, Viollet B, Walsh MP, Hue L & Rider MH (2008). AMP-activated protein kinase phosphorylates and desensitizes smooth muscle myosin light chain kinase. *J Biol Chem* **283**, 18505–18512.

Hue L & Rider MH (2007). The AMP-activated protein kinase: more than an energy sensor. *Essays Biochem* **43**, 121–137.

Jørgensen SB, Viollet B, Andreelli F, Frøsig C, Birk JB, Schjerling P, Vaulont S, Richter EA & Wojtaszewski JF (2004). Knockout of the alpha2 but not alpha1 5′-AMP-activated protein kinase isoform abolishes 5-aminoimidazole-4-carboxamide-1-beta-4-ribofuranoside but not contraction-induced glucose uptake in skeletal muscle. *J Biol Chem* **279**, 1070–1079.

Kahn BB, Alquier T, Carling D & Hardie DG (2005). AMP-activated protein kinase: ancient energy gauge provides clues to modern understanding of metabolism. *Cell Metab* **1**, 15–25.

Lowry OH, Rosebrough NJ, Farr AL & Randall RJ (1951). Protein measurement with the Folin phenol reagent. *J Biol Chem* **193**, 265–275.

Lytle C (1997). Activation of the avian erythrocyte Na-K-Cl cotransport protein by cell shrinkage, cAMP, fluoride, and calyculin-A involves phosphorylation at common sites. *J Biol Chem* **272**, 15069–15077.

Pasini EM, Lutz HU, Mann M & Thomas AW (2010). Red blood cell (RBC) membrane proteomics – Part II: Comparative proteomics and RBC patho-physiology. *J Proteomics* **73**, 421–435.

Pedersen SF, O'Donnell ME, Anderson SE & Cala PM (2006). Physiology and pathophysiology of Na^+/H^+ exchange and Na^+-K^+-$2Cl^-$ cotransport in the heart, brain, and blood. *Am J Physiol Regul Integr Comp Physiol* **291**, R1–25.

Piechotta K, Lu J & Delpire E (2002). Cation chloride cotransporters interact with the stress-related kinases Ste20-related proline-alanine-rich kinase (SPAK) and oxidative stress response 1 (OSR1). *J Biol Chem* **277**, 50812–50819.

Richardson C & Alessi DR (2008). The regulation of salt transport and blood pressure by the WNK-SPAK/OSR1 signalling pathway. *J Cell Sci* **121**, 3293–3304.

Richardson C, Rafiqi FH, Karlsson HK, Moleleki N, Vandewalle A, Campbell DG, Morrice NA & Alessi DR (2008). Activation of the thiazide-sensitive Na^+-Cl^- cotransporter by the WNK-regulated kinases SPAK and OSR1. *J Cell Sci* **121**, 675–684.

Roskoski R Jr (1983). Assays of protein kinase. *Methods Enzymol* **99**, 3–6.

Sanders MJ, Ali ZS, Hegarty BD, Heath R, Snowden MA & Carling D (2007). Defining the mechanism of activation of AMP-activated protein kinase by the small molecule A-769662, a member of the thienopyridone family. *J Biol Chem* **282**, 32539–32548.

Steinberg GR & Kemp BE (2009). AMPK in health and disease. *Physiol Rev* **89**, 1025–1078.

Sugden C, Crawford RM, Halford NG & Hardie DG (1999). Regulation of spinach SNF1-related (SnRK1) kinases by protein kinases and phosphatases is associated with phosphorylation of the T loop and is regulated by 5′-AMP. *Plant J* **19**, 433–439.

Vitari AC, Deak M, Morrice NA & Alessi DR (2005). The WNK1 and WNK4 protein kinases that are mutated in Gordon's hypertension syndrome phosphorylate and activate SPAK and OSR1 protein kinases. *Biochem J* **391**, 17–24.

Vitari AC, Thastrup J, Rafiqi FH, Deak M, Morrice NA, Karlsson HK & Alessi DR (2006). Functional interactions of the SPAK/OSR1 kinases with their upstream activator WNK1 and downstream substrate NKCC1. *Biochem J* **397**, 223–231.

Witters LA, Kemp BE & Means AR (2006). Chutes and Ladders: the search for protein kinases that act on AMPK. *Trends Biochem Sci* **31**, 13–16.

Woods A, Vertommen D, Neumann D, Türk, R, Bayliss J, Schlattner U, Wallimann T, Carling D & Rider MH (2003). Identification of phosphorylation sites in AMP-activated protein kinase (AMPK) for upstream AMPK kinases and study of their roles by site-directed mutagenesis. *J Biol Chem* **278**, 28434–28442.

Author contributions

B.S. conducted most of the experimental work and was involved in conception and design, analysis and interpretation of the data and drafting the article. L.M. carried out some immunoblot and statistical analyses. D.V. carried out phosphorylation site identification by mass spectrometry. B.V. provided AMPKα1-deficient mice and was involved in critically revising the manuscript for final approval. M.R. was responsible for conception and design, interpretation of data and drafting the article. All work was performed in the laboratory of M.R., de Duve Institute, Brussels.

Acknowledgements

We thank Marie-Agnès Gueuning and Nusrat Hussain for their expert technical assistance, Dr Pierre-Paul Prevot for help with animal procedures and Prof. Louis Hue for critically reading the manuscript. The help of Prof. Dario Alessi, for freely providing reagents to carry out the work, is also gratefully acknowledged. Lastly, we thank Prof. Grahame Hardie for production of the anti-phospho Ser77 and anti-phospho Ser242 antibodies in sheep within the framework of the EXGENESIS Consortium. The work was supported by the Interuniversity Attraction Poles Program – Belgian Science Policy (P6/28), the 'Action de Recherche Concertée', Université catholique de Louvain, the Fund for Medical Scientific Research (Belgium) and the EXGENESIS Integrated Project (LSHM-CT-2004-005272) from the European Commission.